NANO LETTERS
Cite This: Nano Lett. 2019, 19, 2588−2597
Letter
pubs.acs.org/NanoLett

Dion−Jacobson Two-Dimensional Perovskite Solar Cells Based on Benzene Dimethanammonium Cation

Bat-El Cohen,[†] Yiming Li,[‡] Qingbo Meng,[‡,§] and Lioz Etgar*[,†]

[†]Institute of Chemistry, The Center for Nanoscience and Nanotechnology, Casali Center for Applied Chemistry, The Hebrew University of Jerusalem, Jerusalem 91904, Israel

[‡]Key Laboratory for Renewable Energy (CAS), Beijing Key Laboratory for New Energy Materials and Devices, Institute of Physics, Chinese Academy of Sciences (CAS), Beijing 100190, P.R. China

[§]School of Physical Sciences, University of Chinese Academy of Sciences, Beijing 100049, P.R. China

Supporting Information

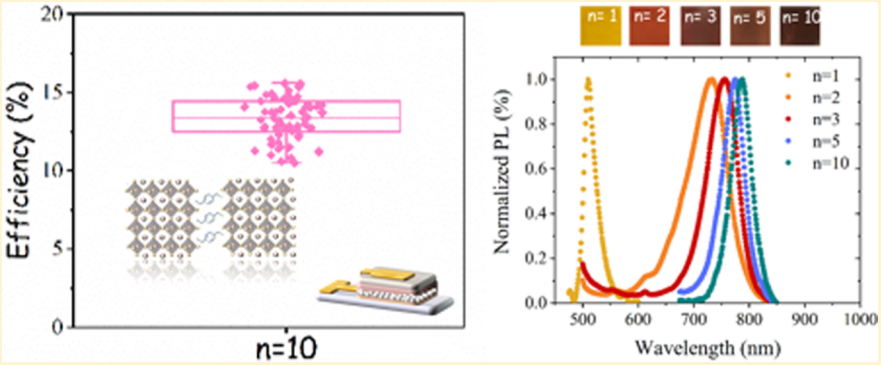

ABSTRACT: Organic−inorganic perovskite structured compounds have recently emerged as attractive materials in the fields of photovoltaic due to their exciting optical properties and easy syntheses, as well as exceptional structural and optical tunability. This work presents a Dion−Jacobson two-dimensional (2D) perovskite using diammonium as the barrier molecule. We show that the diammonium barrier molecule is responsible for the perovskite layers' orientation supported by Hall Effect measurements, which results in a high efficiency solar cell for 2D perovskite without the need for additives or any additional treatment. The 2D perovskite cells achieved an efficiency of 15.6%, which was one of the highest reported for low-dimensional perovskite. Charge extraction, voltage decay, and charge collection efficiency measurements show the beneficial alignment of the 2D perovskites related to the selective contacts. Stability characterization shows that the stability for the 2D perovskite was enhanced compared with their 3D counterparts.

KEYWORDS: *Perovskite, solar cells, two-dimensional perovskite, optoelectronics, renewable energy, stability of PSCs*

In 2009 Miyasaka et al.[1] introduced organic−inorganic perovskite as an absorber for solar cells, achieving a power conversion efficiency (PCE) of 3.8%. Since then, perovskite solar cells (PSCs) have attracted much attention owing to their promising optical and electronic properties, low exciton binding energy, long carrier diffusion length, and simple fabrication methods.[2−7] Today, PSCs are one of the most promising PV technologies, approaching a PCE of 23.3%.[8] The most common perovskite used today as a light harvester in solar cells is three-dimensional (3D) organic−inorganic perovskite with the empirical formula AMX_3, where A is a monovalent organic cation, M is a divalent metallic cation, and X is a monovalent anion. In this perovskite structure, the inorganic part consists of a corner-sharing MX_6 octahedral, where the organic cation is localized inside the octahedral cage. In order to form the 3D structure of the perovskite, the organic cation should be small enough to enable adding another corner-sharing MX_6 octahedral.

The two-dimensional (2D) perovskite is a closely related structure. Here the small organic cation is replaced by a large organic cation, which does not fit into the octahedral cage. In this case, the inorganic framework will be separated by a long organic cation, where van der Waals interactions are present between the organic molecules.[9,10] The long organic ammonium barrier forms a layer having a low dielectric constant ∼2.4, whereas the metal halide layers possess a high dielectric constant of more than 6. Thus, the 2D perovskite structure can be referred to as a periodic array of quantum wells.[11,12] Regarding the quantum-well model, it is expected to have 2D perovskite properties that differ from those of 3D perovskite. The 2D perovskite exhibits a wide band gap, a high exciton binding energy, and low carrier mobility (for

Received: January 27, 2019
Revised: March 3, 2019
Published: March 11, 2019

DOI: 10.1021/acs.nanolett.9b00387
Nano Lett. 2019, 19, 2588−2597

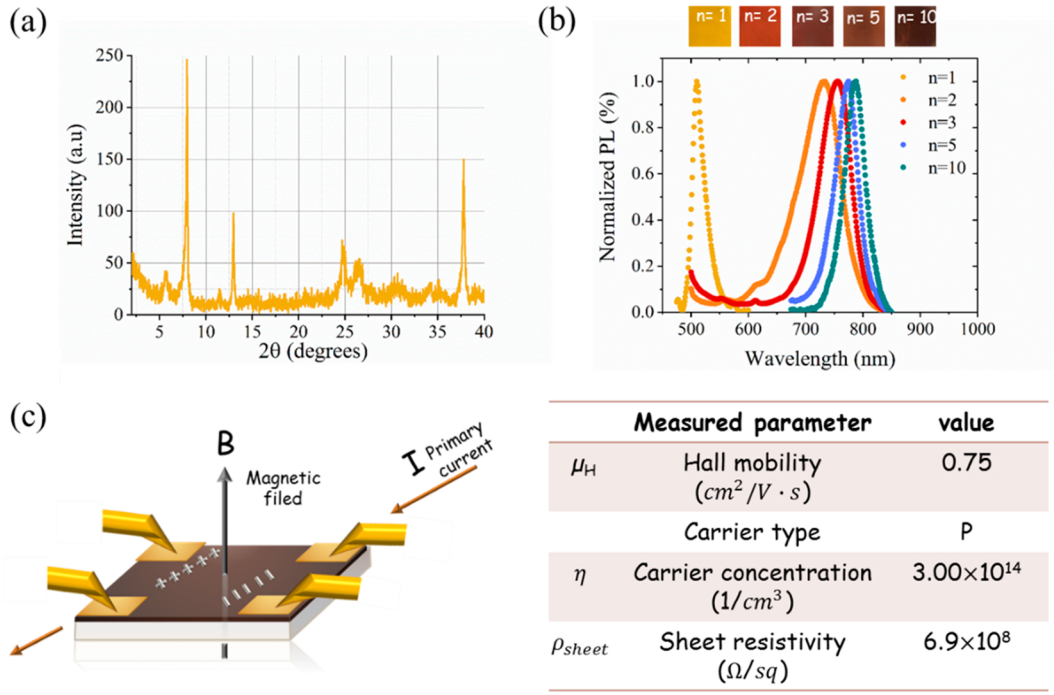

	Measured parameter	value
μ_H	Hall mobility $(cm^2/V \cdot s)$	0.75
	Carrier type	P
η	Carrier concentration $(1/cm^3)$	3.00×10^{14}
ρ_{sheet}	Sheet resistivity (Ω/sq)	6.9×10^{8}

Figure 1. (a) The XRD diffraction pattern for pure 2D perovskite (n = 1); the peaks at ~5.7° and ~7.9° are related to the zigzag structure of the perovskite. (b) The PL and photos of 2D perovskite films at various n values. (c) Schematic illustration of Hall Effect measurement (left) and the measured parameters by the Hall Effect of n = 10 BzDAI-based perovskite (right).

unorganized perovskite layers), which makes it challenging to function as a light harvester in the solar cell.[13−17] When combining both small and long organic cations, intermediate states are formed, where stacks of organic−inorganic perovskite layers are periodically separated by long organic molecules. This perovskite structure has the formula $(R\text{-}NH_3)_2A_{n-1}M_nX_{3n+1}$, where R-$NH_3$ is the long organic cation, n is the number of confined inorganic layers between the long organic cations, and A is the small organic cation that fits into the octahedral cage.[9,18−20] The formation of this layered perovskite is determined by the stoichiometric ratio of the precursors. Previous studies showed that for a single crystal with $n \leq 4$ the number of inorganic framework layers is in good agreement with the n value, whereas at n = 5 only 90% purity was found for specific perovskite structures.[19]

One of the interesting properties of 2D perovskite is its resistivity to humidity.[21−23] By combining both small and long organic cations, one can achieve better stability with 2D perovskite along with the excellent optical and physical properties of 3D perovskite.

In 2014 Smith et al.[21] conducted for the first time experiments with quasi-2D perovskite ($(R\text{-}NH_3)_2A_{n-1}M_nX_{3n+1}$ where $n > 2$) as an active layer in PSC and achieved a PCE of 4.7%. The key to achieving a high PCE in quasi-2D perovskite-based solar cells is to organize the layers on the substrate. The inorganic framework on the substrate is organized when the organic cations (barriers) are perpendicular to the substrate; this enables efficient charge transport through the perovskite. Recently, Tsai and co-workers[24] reported on a hot casting method for a planar PCS that improves the arrangement of the quasi-2D perovskite on the surface. As a result, a PCE of 12.5% was achieved for the perovskite $(BA)_2(MA)_3Pb_4I_{13}$ (BA = butyl ammonium, MA = methylammonium). Sargent et al.[23] demonstrated quasi-2D perovskite with high n values and achieved a high PCE with enhanced stability; however, owing to the high n values, a mixture of 3D perovskite with 2D perovskite was formed.

In our previous work, we showed that when high n values are used in quasi-2D perovskite, high efficiency, high voltage, and enhanced stability of the cells can be achieved.[25,26] Further reports showed that 2D/3D perovskite was used as the active layer in PSCs displaying efficiencies comparable to the 3D PSCs but with improved stability.[27−36]

In this work, we present a diammonium cation as the barrier molecule to achieve a Dion−Jacobson 2D perovskite, resulting in highly efficient 2D perovskite solar cells achieved without the need for additives or pretreatment. We performed full characterizations on films and complete cells in order to study the optical, physical, and electrochemical properties of these cells. In addition, different stability measurements were performed under illumination and humidity conditions.

Results and Discussion. In a two-dimensional perovskite where the long organic cation has one ammonium functional group, it can interact with the inorganic framework and the other long organic cations by van der Waals interactions. However, when using an organic cation with two ammonium functional groups, i.e., diammonium cations, then the inorganic framework is held together by one molecule, meaning by ionic interactions.[9,21,22,37,38] Since ionic bonds are stronger than van der Waals interactions,[39−42] it is expected that the layered perovskite will be organized better. Organizing the perovskite's layers will enhance the charge transport through the 2D perovskite film. Therefore, it can be expected that at low n values one can observe high efficiency with a very stable solar cell using the diammonium cation as the barrier molecule.

Recently a comparison was reported[30] between quasi-2D perovskite based on mono- and di- ammonium cations, i.e., butyl ammonium and butyl diammonium, as the "barrier" molecules. It was found that perovskite based on a butyl diammonium barrier exhibits better crystal orientation than the

DOI: 10.1021/acs.nanolett.9b00387
Nano Lett. 2019, 19, 2588−2597

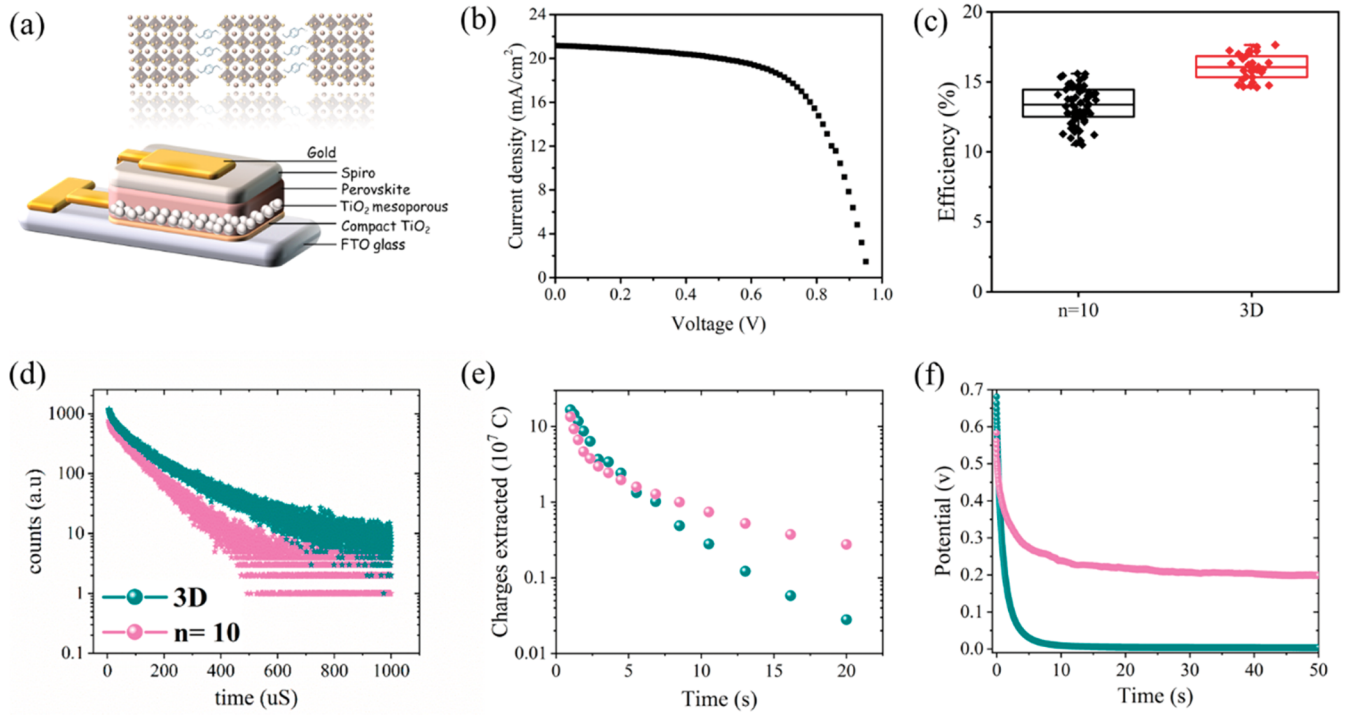

Figure 2. (a) Schematic illustration of the perovskite solar cell configuration used in this work and the organization of the perovskite layers on the substrate. (b) A J–V curve of the best efficiency 2D (n = 10) PSC. (c) Statistical data of PCE for 2D and 3D PSCs. (d) PL decay for perovskite films (glass substrate), (e) charge extraction, and (f) voltage decay measurements for PSCs, pink for 2D (n = 10) perovskite and green for 3D perovskite.

butyl ammonium barrier; thus it generates better photovoltaic (PV) performance. Despite the improvement in the PCE of the solar cells with a diammonium barrier, the PCE of low-dimensional perovskite (low n values) remains challenging. In this work we developed PSCs using 2D perovskite with the chemical formula $(NH_3\text{-R-}NH_3)A_{11}M_{12}X_{37}$, using 1,4-benzenedimethanamonium iodide (BzDAI) as a barrier molecule (the barrier molecule's structure and a schematic illustration of the perovskite layers using this barrier are shown in Figure S1 in the Supporting Information). We chose this barrier molecule because of (i) the diammonium functional group, which should provide a more organized structure; (ii) the relatively short length of the molecule, which will decrease the distance between the inorganic framework; (iii) the aromatic ring, which should have free π-electrons; therefore, it can enhance the charge transport.

The use of a diammonium cation as a barrier in 2D perovskite has been characterized before.[18,38,43−45] It was shown that a zig- zag morphology is formed with ⟨001⟩ and ⟨110⟩ crystallographic planes. An X-ray diffraction (XRD) pattern for $(BzDA)Pb(I_{0.93}Br_{0.07})_4$ (n = 1, BzDA- 1,4-benzenedimethanamonium) can be observed in Figure 1a, demonstrating the ⟨001⟩ and ⟨110⟩ crystallographic planes at ∼5.7° and ∼7.9°, respectively, indicating the formation of the zigzag structure in 2D perovskite. The dominant peak at ∼5.7° corresponds to d-spacing of ∼11.1A, whereas the low intensity peak at ∼7.9° corresponds to d-spacing of ∼15.4A.

The dimensionality of the perovskite was first characterized by absorbance and photoluminescence (PL). Figure S2 shows the absorbance onset while the n value is increased. For n = 1 the absorbance onset is about 530 nm, and when it is increased to n = 2, a typical excitonic peak is revealed, which indicates the low dimensionality of the perovskite.[11,12,22,25,26] Increasing the n value results in a red shift of the absorbance onset until a 3D perovskite wavelength of 800 nm is reached. Similarly, the PL is red-shifted while tuning the dimensionality of the perovskite, as can be seen in Figure 1b. The PL spectra reveal a slight red shift between n = 5 and n = 10, which cannot be observed by the absorbance spectra. This shows that also when n = 5 to n = 10 the perovskite's dimensionality takes place. The full wide half-maximum (fwhm) of the PL peaks as a function of the n values, which is presented in Figure S2. With pure 2D perovskite (n = 1), the fwhm is narrow, indicating a pure phase where n = 1 in the perovskite film. Increasing the n value to n = 2 results in a more than 60 nm increase in the fwhm of the PL, which suggests that already at n = 2 the n values are mixed inside the film. However, interestingly, a further increase in the n value results in a decrease in the fwhm, which shows the effect of 1,4-benzenedimethanamonium iodide (BzDAI) as a barrier molecule by creating more organized layers of perovskite even at higher n values. (i.e., less distribution of different n values inside the perovskite film).

As discussed earlier, the pure 2D perovskite (n = 1) could not be used as an efficient light harvester in the solar cell. Therefore, we increased the perovskite dimensions by adding small organic cations. In this work mixed small cations were used, namely, formamidinium (FA^+), methylammonium (MA^+), and cesium (Cs^+) at a ratio of 0.80:0.15:0.05, respectively.

We found that the optimum composition with the largest amount of barrier molecule in solution and that delivers the best PV performance is $(BzDA)\text{-}(Cs_{0.05}MA_{0.15}FA_{0.8})_9Pb_{10}(I_{0.93}Br_{0.07})_{31}$, n = 10. To make it simple, we will assign the small cations as "A", i.e., $(BzDA)A_9Pb_{10}(I_{0.93}Br_{0.07})_{31}$. Lower n values of perovskites result in a variety of inactive phases of FA^+- and Cs^+-based

DOI: 10.1021/acs.nanolett.9b00387
Nano Lett. 2019, 19, 2588−2597

perovskites. It was reported that the black photoactive phase of $FAPbI_3$ at a high purity even with the addition of small cations such as Cs^+ and MA^+, is challenging to observe.[46] We found that for low n values (higher amounts of barrier molecule), as well as for 3D perovskite, additional inactive photovoltaic phases appeared, whereas in the case of n = 10 almost only pure phases were observed. Figure S2a shows the XRD spectra of additional phases that were formed when n = 5 and with 3D perovskite and the pure phase when n = 10. Stabilization of $FAPbI_3$ and $CsPbI_3$ by 2D perovskite have been reported;[47−50] however, high PCE cannot be achieved when the concentration of the barrier molecules is high. One way to achieve both phase stabilization and high PCE is by using the diammonium cation as the barrier molecule.

The $(BzDA)A_9Pb_{10}$ $(I_{0.93}Br_{0.07})_{31}$, n = 10, 2D perovskite was used to prepare PV solar cells. A standard mesoporous configuration of PSCs was used, as illustrated in Figure 2a. The perovskite was deposited by a stoichiometric amount of the precursors as described in more detail in the experimental section. In order to confirm the ratio between the small and the long organic cations in the already deposited perovskite film, analytic H NMR was used. The perovskite was scratched from the substrate after deposition and taken for analytic H NMR measurement. By integrating the peak of the protons, the ratio between the small and the long organic cations can be observed. Figure S3 shows the H NMR spectrum, where the ratio between formamidinium and BzDA is about 1:10 (e.g., n = 11); by considering the other additional small cations in the perovskite, we can predict that the actual n value of the perovskite is about 12. Although this measurement shows us the ratio between the organic cations, it cannot provide us with the specific organization of the 2D perovskite layers.

The Hall Effect measurements were applied on the n = 10 2D perovskite in order to measure the hall mobility. In this measurement the perovskite is deposited on a glass substrate where four gold contacts are evaporated on the corners of the substrate as can be seen in Figure 1c (the complete experimental details are available in the Supporting Information). In order to estimate the photocurrent behavior, the samples were measured in the dark, and under illumination. The dark measurements showed high resistivity in the range of the instrument detection limit while during illumination (0.25 sun) the sheet resistance decreased in about 2 orders of magnitude than in the dark 6.9 × 108 (Ω/sq). The perovskite shows a p-type behavior with a carrier concentration of 3.00 × 10^8 $1/cm^3$ and Hall mobility of 0.75 $cm^2/V{\cdot}s$ which is comparable to different types of 3D perovskite with similar or higher illumination intensities.[51,52] This suggests that the 2D perovskite based on the BzDA barrier provides a sufficient organization of the perovskite's layers.

An interesting observation is the deposition of 2D perovskite versus 3D perovskite. With 2D perovskite, the deposition appeared to be very smooth and repeatable, and a mirror-like perovskite was formed and apparently the deposition was less sensitive to the specific hand skills of the operator as opposed to the case of standard 3D perovskite, which is well-known for its repeatable problems.[53] The top view scanning electron microscope (SEM) images (Figure S4) show a smooth and pinhole-free surface for 2D perovskite; this observation was also supported by the atomic force microscope (AFM) measurements (Figure S5), which show a root mean square (RMS) of 26.7 nm for 2D perovskite and 30.7 nm for 3D perovskite. The top view SEM image for n = 1 2D perovskite shows a rod-shaped crystal. The cross-section SEM images (Figure S4) of n = 1 shows nonoriented platelet crystals, whereas 3D and 2D perovskites show dense and defined crystals.

The best PV performance was achieved for 2D (n = 10) PSC, which displayed a PCE of 15.6%, an open circuit voltage (V_{oc}) of 1.02 V, a short circuit current density (J_{sc}) of 21.5 mA/cm^2, and a fill factor of (FF) 71%. The $J-V$ curve of this recorded cell can be seen in Figure 2b. Figure 2c presents the statistical data of 97 fabricated cells for 2D and 3D PSCs, where each solar cell has one pixel for measurement. It can be seen that the average PCE of 2D PSCs approach the average PCE of the 3D cells, and even some of the 2D PSCs exceed the efficiencies produced by the 3D PSCs. Figure S6 presents the statistical data for all the PV parameters (V_{oc}, J_{sc}, and FF). The 2D PSCs produced relatively high PV parameters and the average values are as follows: a J_{sc} of 20.0 mA/cm^2, a V_{oc} of 1.03 V, and a FF of 63%, which can support an organized layered structure inside the 2D perovskite. Previous reports indicated that high current density cannot be achieved in 2D perovskite without arranging the orientation of the layers.[24,33,54] In this work, a high current density of more than 20 mA/cm^2 was achieved for low-dimensional perovskite without any additives or special deposition methods. Therefore, it can be concluded that the diammonium barrier (BzDA) molecule is responsible for the orientation of the layers inside the perovskite film. A schematic illustration of the layers' orientation using the barrier molecules of BzDA, compared to the case of the monoammonium functional group as the barrier molecules, can be seen at the inset of Figure 2a and Figure S7. The current as a function of time was measured (Figure S8) to show the steady state of these cells. It takes more time for the 2D PSCs compared with the 3D PSCs to reach steady state. When observing the $J-V$ curves of 2D PSC before and after approaching steady state conditions (Figure S9) and its specific PV parameters (Table S1), it can be seen that the FF is the most influential factor before and after achieving steady-state conditions. In previous studies on $MAPbI_3$ PSCs,[55,56] it was observed that when the cells were measured without any pretreatment, a slight s-shape appeared in their $I-V$ curves; this s-shape diminishes over time during illumination and with applied bias. This phenomenon can be related to the diffusion of ionic species[57−59] or the orientation of the organic cations[57,60,61] in the perovskite. Therefore, it is not surprising that this effect is pronounced in the 2D perovskite, and it may also suggest that the 2D perovskite has a slower diffusion of ions.

The PL lifetime was measured for 2D and 3D perovskite films, as can be seen in Figure 2d. The PL lifetime was longer for 3D perovskite (τ_2 = 157 μs) than for 2D (τ_2 = 86 μs). The longer lifetime for 3D perovskite is due to the confined layers of the 2D perovskite and the barriers inside this structure that inhabit the lifetime of the carriers.

Charge extraction measurements were performed to better understand the electronic properties of this low-dimensional perovskite solar cell. Charge extraction measurements were previously used to characterize the recombination rate in the dye-sensitized solar cell and PSCs.[25,62,63] Briefly, the measurement consists of a few steps: (1) the cell is disconnected and illuminated for 2 s (white LED, ∼0.7 sun), (2) the cell stays in the dark for a certain period of time (delay time), which changes from measurement to measurement, (3) the cell is

DOI: 10.1021/acs.nanolett.9b00387
Nano Lett. 2019, 19, 2588−2597

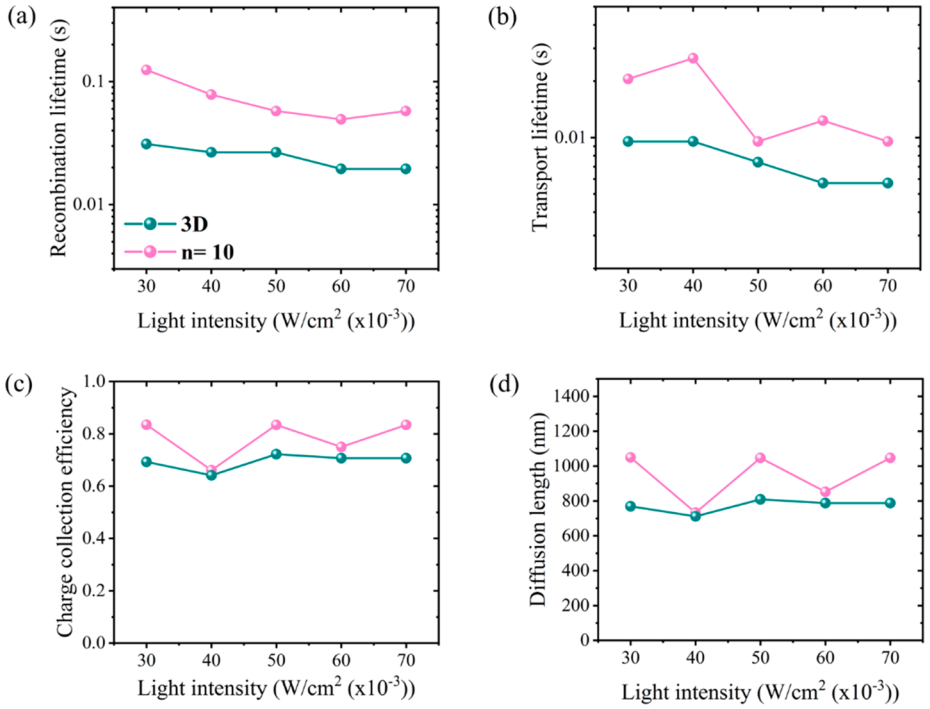

Figure 3. (a) Electron recombination lifetime (extracted from IMVS measurements. (b) The transport lifetime (extracted from IMPS measurements, (c) charge collection efficiency, and (d) diffusion length as a function of light intensities for 2D PSC and 3D PSC in pink and green, respectively.

connected and the charges that are left are extracted from the cell. During the time in the dark the charges have time to move inside the cell or to recombine. At any given time, if more charges are left to extract, this indicates that fewer charges have been recombined during the delay time. This measurement is mainly related to the recombination rate and the traps at the perovskite and at the interface between the absorbing materials and the selective contacts. Although the PL decay for 2D perovskite film was shorter than for the 3D, the charge extraction for 2D PSCs is longer than for 3D (Figure 2e). This suggests a lower recombination rate at selective contacts for 2D PSCs, meaning a better alignment of the electronic properties between the 2D perovskite and the selective contacts.

In order to further elucidate the recombination behavior in these cells, voltage decay measurements were performed. In voltage decay measurements, the cell is illuminated with white LED (~0.7 sun) for 2 s, allowing the potential to build up. In the next step, the cell is left in the dark and the decay time of the potential is recorded. Figure 2f shows the decay of the potential in the dark for 2D and 3D PSCs. Two main points can be concluded from this measurement: (1) 2D and 3D PSC have different decay times and (2) there is a buildup of electrostatic potential for 2D PSC. As can be seen, the potential decay for 2D PSC is slower than for 3D PSC (this can be seen clearer in Figure S10), which suggests a faster recombination rate for 3D than for 2D.

In addition, it can be observed that some potential is left after a long time in the dark for 2D PSC (Figure 2f). This can be attributed to the buildup of electrostatic potential, which is equal to ~250 mV, whereas with 3D PSC the buildup electrostatic potential drops to zero. A previous study[64] conducted on $MAPbI_3$ PSCs analyzed the behavior of voltage decay in PSCs under different conditions. This study attributed the formation of electrostatic potential to an accumulated region inside the perovskite layer (caused by ion migration), which results in inner electrostatic potential. The additional electrostatic potential adds to the standard buildup in potential, increasing the overall voltage of the cell. Furthermore, this inner potential supports the longer separation of charges in the perovskite layer. Both charge extraction and voltage decay support the observation of a lower recombination rate near the selective contacts, suggesting that a better alignment exists between the 2D perovskite and the selective contacts.

Intensity-modulated photocurrent and photovoltage spectroscopies (IMPS/IMVS) were used to electrochemically characterize the cells. The time constants for the electron recombination lifetime (τ_r) and the electron transport (τ_t) lifetimes were obtained from the inverse of the minimum angular frequency (ω_{min}) in the IMPS and IMVS spectra. Figure S11 shows the representative IMVS and IMPS spectra for 2D and 3D PCS, from which the minimum frequency was extracted.

The electron recombination lifetime τ_r was found to be longer for 2D PSC than for 3D PSC (Figure 3a), which is in good agreement with the CE and voltage decay, which showed a reduced recombination rate at the contacts. Figure 3b presents the electron transport lifetime, and as expected, the electron transport lifetime decreases with the light intensity. When comparing the electron transport lifetimes of 2D and 3D PSC, the 2D perovskite exhibited a longer electron transport lifetime than did the 3D perovskite. The longer electron transport lifetime could be related to the barrier molecules present in the 2D perovskite structure.

Importantly, as long as the transport lifetime is longer than the recombination lifetime, the solar cell can generate current and voltage. This is defined as the charge collection efficiency,

DOI: 10.1021/acs.nanolett.9b00387
Nano Lett. 2019, 19, 2588−2597

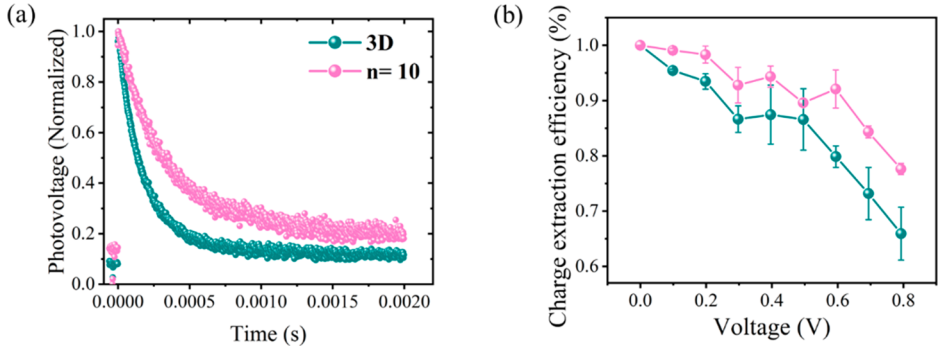

Figure 4. (a) Normalized photovoltage results from TPV measurements, (b) the average normalized charge extraction efficiencies calculated with $\Delta V/\Delta V$ (0 mV), where ΔV is the peak of the TPC decay curves at different bias voltages for 2D PSC and 3D PSC, shown in pink and green, respectively.

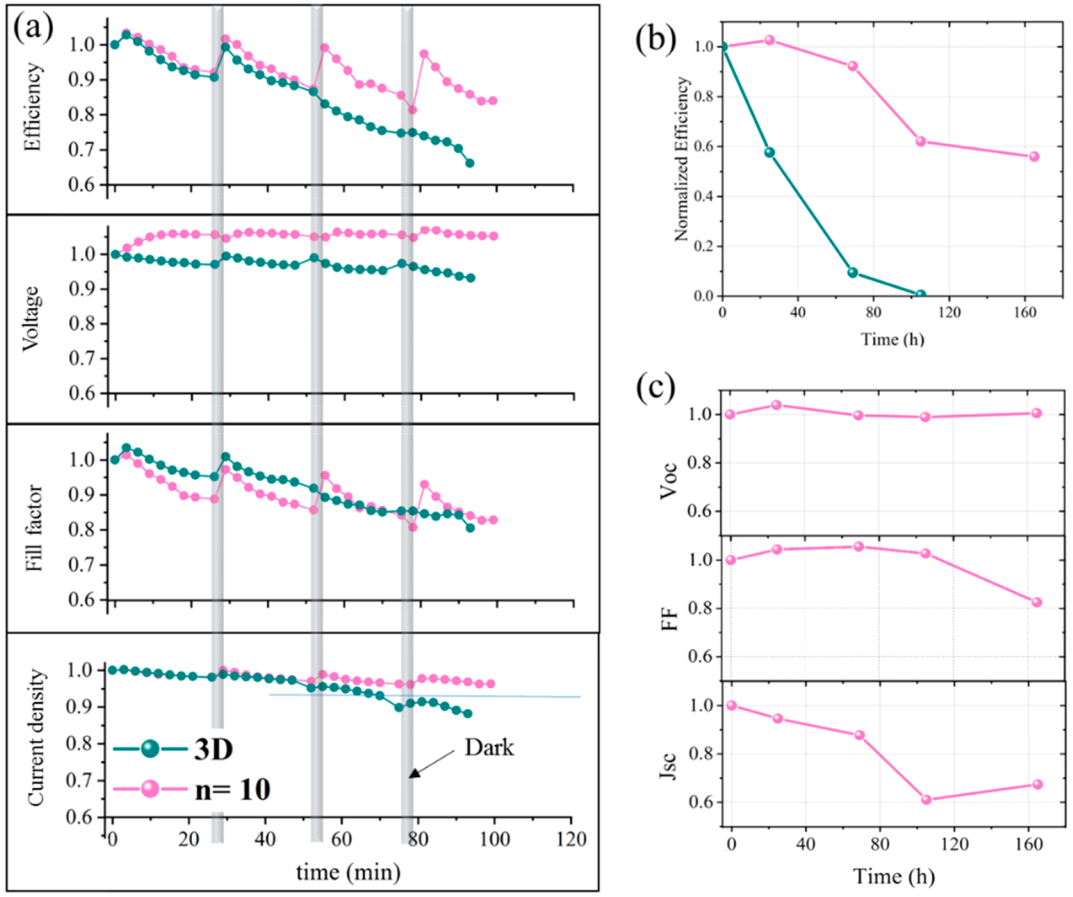

Figure 5. (a) Stability measurements: Continuous 1 sun illumination for 22 min followed by 5 min in the dark; the whole stability measurement took 100 min. V_{max} was applied on the cell in the dark. (b) Stability measurements under ambient air (up to 50% relative humidity) for nonencapsulate PSCs, and (c) the corresponding PV parameters of the cell presented in b. Pink represents 2D PSC and green represents 3D PSC.

as can be seen in Figure 3c. The charge collection efficiency is calculated using $\eta_{cc} = 1 - \tau_t/\tau_r$. The 2D PSC achieves a charge collection efficiency of 0.8−0.9 for the whole range of light intensities better than does the 3D PSC, which approaches a charge collection efficiency of 0.7. The high charge collection efficiency with 2D PSC indicates that 2D perovskite has a beneficial alignment with the selective contacts. This was further supported by charge extraction and voltage decay measurements as described above. The higher charge collection efficiency and the longer recombination lifetime of 2D perovskite in comparison with 3D perovskite shows a potential of 2D PSCs to gain higher efficiencies than do the 3D PSCs in the future owing to better alignment of the 2D perovskite properties to the selective contacts.

The electron diffusion length can be calculated using the IMVS and IMPS data according to the equation,[65−68] $L_d = \sqrt{D\tau_r}$, where D is the diffusion coefficient calculated from τ_t and represents the thickness of the absorber layer. Figure 3d presents the diffusion length as a function of the light intensity. The 2D PSCs display a diffusion length in the range of ∼800−1100 nm, whereas the 3D PSCs display a diffusion length of ∼800 nm. The long diffusion length observed with 2D PSC could be related to the diammonium

DOI: 10.1021/acs.nanolett.9b00387
Nano Lett. 2019, 19, 2588−2597

barrier molecule that prolonged the electron recombination lifetime and the diffusion coefficient due to the accumulation of carriers at the benzene ring.[69]

To further evaluate the difference in charge recombination dynamics between 3D and 2D PSCs, transient photovoltage (TPV) measurements were employed.[70,71] Figure 4a presents the TPV results of the 3D and n = 10 samples under zero bias voltage. The curves were fitted by a single-exponential decay function. The recombination lifetime for 3D perovskite is shorter than that of 2D perovskite (n = 10). A long lifetime indicates less charge recombination and trap density,[72] which agrees well with the IMVS results. In addition to the charge recombination property, charge extraction dynamics is also studied by the modulated transient photocurrent (M-TPC) method.[71] Figure S12 shows the M-TPC results of a 3D PSC and a 2D PSC under bias voltages ranging from 0 to 800 mV.

The charge extraction efficiencies were calculated when comparing the peak photocurrent at different bias voltages for the 3D and the 2D (n = 10) cells, as presented in Figure 4b. When a bias voltage is applied on PSC, the charge extraction is less efficient due to the decrease in the built-in electric field and the increase in both bulk and interfacial recombination in the perovskite layer. Under applied bias voltages, the n = 10 PSC displays much better charge extraction efficiency than that of the 3D PSCs, indicating its superior operational stability continuously measured at applied biases.[72] These results are consistent with the charge extraction, as well as the IMVS and IMPS measurements, which indicate that 2D perovskite has very good electronic and energy level alignment.

The stability of the cells was studied using two independent measurements. Figure 5a shows the PV parameters of the cells (2D and 3D PSCs) under continuous 1 sun illumination for 25 min, followed by 5 min in the dark where the cells were held at V_{max}. This measurement lasted for over 100 min. It can be observed that the 2D PSC can recover better than the 3D PSC after being in the dark for 5 min each time. The 3D PSC recovered just after the first 5 min cycle in the dark; thereafter, the efficiency dropped continuously. However, 2D PSC is completely the opposite, where a recovery can be seen after each cycle in the dark. After the third cycle in the dark (i.e., 80 min), the 2D PSC exhibited about 97% of its initial efficiency, whereas the 3D PSC dropped to 75% of its initial efficiency. The current density and the open circuit voltage remain almost constant for 2D PSC, whereas for 3D PSC these parameters are reduced by around 10%. The FF is reduced in both cells by about 15% from their initial FF; also in this case the 2D PSC recovers after each cycle in the dark. To sum up, the 2D PSC exhibits much better stability and recovery properties than does the 3D PSC, which can be explained by its barrier molecule, which enhances its stability. This is further supported by the additional stability measurements under ambient air for nonencapsulated cells (Figure 5b,c). Here, the solar cells were kept in the dark in ambient air with 20%−50% humidity for 160 h (around a week). Figure 5b,c presents the normalized PV parameters over a week. The 2D PSC exhibits better stability also in this case, as expected, owing to its long organic barrier in the perovskite structure. The efficiency of 2D PSC dropped to 80% of its initial efficiency after 84 h, whereas the 3D PSC dropped to this efficiency already after 12 h. Another interesting observation is that after 2 days, the 3D PSC stopped working, whereas the 2D PSC still displayed 60% of its initial efficiency. The other PV parameters can be seen in Figure 5c, where the reduction in the J_{sc} value is responsible for the drop in the efficiency. Interestingly, in the case of the stability under illumination, the reduction in the FF was responsible for the drop in the efficiency, which suggests that different degradation processes exist under humidity and under illumination. In conclusion, the 2D PSCs exhibit enhanced stability under illumination and under humidity better than the 3D PSCs do.

Methods. *Material Synthesis.* 1,4-Benzenedimethanamonium iodide was synthesized by dissolving 5 g of p-xylylenediamine (99% Sigma) in 20 mL of ethanol absolute and reacting it slowly while stirring with 20 mL of hydroiodic acid (57 wt % in water, Sigma); the reaction was performed in an ice bath. After the addition of acid, the precipitate was left for 20 min. The precipitate was then washed repeatedly three times with diethyl ether and recrystallized twice with ethanol absolute.

Preparation of Perovskite Solutions. The perovskite solutions were prepared in a nitrogen-filled glovebox H_2O < 0.1 ppm and O_2 < 5.0 ppm.

All organic precursors were purchased from GreatCell solar and all of the inorganic precursors were purchased from Sigma-Aldrich. A mixture of cation and halide 3D perovskite solution was prepared by dissolving 1.5 mM MABr, FAI, PbI_2, and $PbBr_2$ in a mixture of 1 mL of dimethylformamide: dimethyl sulfoxide (DMF/DMSO) (820:180) with a 1.5 mM concentration. A CsI solution (1.5 mM) was prepared separately by dissolving CsI_2 in DMSO. Next, 50 μL of the CsI solution were added to the perovskite solution to form a 1:3:16 ratio between Cs:MA:FA, and a 9:1 ratio between PbI_2 and $PbBr_2$. $(BzDA)A_9Pb_{10}$, n = 10 2D perovskite solutions were prepared by dissolving stoichiometric amounts of the precursors in 1 mL of a DMF:DMSO mixture (820:190) solution; the 50 μL CsI solution was added to the solution, where the correct ratio between the small cations and the 2D barrier were maintained. The perovskite solutions were prepared 4−5 h before the perovskite deposition.

Device Fabrication. SnO_2/F(FTO) conductive glass (10 O cm1, Pilkington) was etched by reacting zinc powder with concentrated HCl (37% Sigma) on top of the glass, and cleaned thoroughly in sonication bath. After 10 min of argon plasma treatment (60% power, diener), compact TiO_2 (TiDIP, 75% in isopropanol Aldrich diluted 1:5 in isopropanol) was deposited on the substrate by spin coating (5000 rpm 30 min), followed by deposition of m-TiO_2 nanoparticles (30NRD, dyesol) (1:5 w/w% in ethanol absolute) spin-coated at 5000 rpm, 30 s. TiO_2 substrate was treated with Li-TFSI as described elsewhere.[73] Briefly, 1 M of Li-TFSI in acetonitrile was spin coated on a TiO_2 layer at 3000 rpm for 30 s; then the substrate was annealed to 450 °C for 30 min. The substrate was removed from the hot plate at 150 °C directly to a nitrogen filled glovebox (H_2O < 0.1 ppm and O_2 < 5.0 ppm) in the size of 110 × 80 × 60 cm^3 where the perovskite deposition was performed. For the perovskite deposition, 50 μL of perovskite solution was dropped onto the substrate, followed by a spin-coated process having a 5 s delay time, 10 s spin at 1000 rpm, and 45 s spin at 5000 rpm Fifteen seconds before the spin process ended, 100 μL of chlorobenzene (CB) were added dropwise onto the substrate. The films were annealed at 100 °C for 30−40 min. Next, a HTM layer was deposited by 50 μL of 2,2′,7,7′-tetrakis(*N*,*N*-di-4-methoxyphenylamino)-9,9′-spirofluorine (spiro-OMeTAD) in CB (720 mg in 1 mL) containing additives of 17.5 μL of bis(trifl uoromethane)-sulfonimide lithium salt in acetonitrile (520 mg/mL), and 28.8

DOI: 10.1021/acs.nanolett.9b00387
Nano Lett. 2019, 19, 2588−2597

μL of 4-tert-butilpyridine (Sigma) was spin coated at 4000 rpm for 30 s. Finally, a 70 nm thick gold electrode was thermally evaporated on the film under a vacuum of ~10^{-7} Torr. In each set, 12 cells have been fabricated where each cell has single pixel available for measurement.

Absorbance Measurements. Absorbance measurements were performed using a Jasco V-670 spectrophotometer.

Photoluminescence (PL) and Time-Resolved PL Measurements. Steady-state and time-resolved photoluminescence were measured by the PL spectrometer (Edinburgh Instruments, FLS 900) using a pulsed diode laser (EPL-640, ~20 nJ·cm^{-2}/pulse) as the excitation source.

X-ray Diffraction (XRD). X-ray diffraction measurements were performed on a D8 Advance diffractometer (Bruker AXS, Karlsruhe, Germany) with a secondary graphite monochromator, 2° Soller slits, and a 0.2 mm receiving slit. XRD patterns ranging from 2° to 75° 2q were recorded at room temperature using CuKa radiation (l = 1.5418 Å) with the following measurement conditions: a tube voltage of 40 kV, a tube current of 40 mA, a step-scan mode with a step size of 0.02° 2θ, and a counting time of 1 s/step.

Extra High-Resolution Scanning Electron Microscopy (XHRSEM). Magellan XHR SEM was performed using a FEI (field emission instruments), The Netherlands. The measurement conditions were 5 kV

Atomic Force Microscopy (AFM). Scanning probe microscope measurements were made by using Dimension 3100 Nanoscope V in tapping mode.

Charge Extraction, Voltage Decay, and IMVS/IMPS Measurements. Charge extraction and voltage decay measurements were carried out using an Autolab Potentiostat-Galvenostat (PGSTAT) with a FRA32 M LED driver equipped with a white light source. The cells were illuminated from the substrate side. Nova 1.11 software program was used to collect and analyze the data obtained.

Transient Photovoltage/Transient Photocurrent (TPV/TPC). M-TPC/M-TPV measurements, nonequilibrium carriers in the cell, were excited by a 550 nm (Opotek, Radiant 355 LD) pulse laser. A digital oscilloscope (Tektronix, DPO7354C) was used to record the photocurrent or photovoltage decay process with a sampling resistor of 50 Ω or 1 MΩ, respectively. A digital signal generator (Tektronix, AFG 3052C) was used to provide an external modulation to the cell, which is connected in parallel to the signal acquisition circuit. A low-pass filter (LPF) with an inductor (for example, 50 H) and a capacitor (for example, 10 μF) was applied to separate the transient electrical signal from the voltage source to avoid shunting the output.

Hall Effect. Hall Effect measurements were performed using Lake Shore ac/dc Hall Effect system 8404 model. A magnetic field of 1.7 T, and a current of 80 nA were used in the measurement. The samples were illuminated by 0.25 sun of white LED source. Each measurement was conducted 10 times, the average results and the standard deviations were used to the calculation of the final values. It should be mentioned that this measurement is challenging in the case of high resistive materials such as organic semiconductors. Therefore, in this measurement we used an additional high resistivity feature in order to achieve reliable results.

Photovoltaic Characterization. Photovoltaic measurements were using a New Port system, composed of an Oriel $I-V$ test station using an Oriel Sol3A simulator. The solar simulator is class AAA for spectral performance, uniformity of irradiance, and temporal stability. The solar simulator is equipped with a 450 W xenon lamp. The output power is adjusted to match AM1.5 global sunlight (100 mW cm^2). The spectral matched classic cations are IEC60904-9 2007, JIC C 8912, and ASTM E927-05. The $I-V$ curves were obtained by applying an external bias to the cell and measuring the generated photocurrent with a Keithley model 2400 digital source meter.

Conclusions. In this work, we demonstrated high efficiency in 2D perovskite solar cells without any additives or additional treatment to the perovskite. A diammonium cation was used as the barrier molecule in the 2D perovskite, which formed a Dion–Jacobson perovskite structure. The 2D perovskite cells achieved a PCE of 15.6%, an open circuit voltage of 1.02 V, a short circuit current density of 21.5 mA/cm^2, and a fill factor of (FF) 71%, which is one of the highest reported for low-dimensional perovskite. Charge extraction and voltage decay measurements show that the 2D perovskite is better aligned to the selective contacts than the 3D perovskite. This was further supported by the high charge collection efficiency of these cells in the range of 0.8–0.9 for a variety of light intensities. Moreover, the diffusion length of the 2D perovskite was calculated by the IMVS and IMPS techniques, displaying ~800–1100 nm. Finally, the stability of these cells was studied and compared to 3D perovskite cells. It can be concluded that the 2D perovskite-based solar cells are much more stable than their 3D counterparts. This work demonstrates the ability to achieve high efficiency in low-dimensional perovskite solar cells without the need for any additive or additional treatment by choosing the appropriate barrier organic cation.

■ ASSOCIATED CONTENT

Supporting Information

The Supporting Information is available free of charge on the ACS Publications website at DOI: 10.1021/acs.nanolett.9b00387.

XRD, absorbance, NMR, SEM, AFM, and solar cells statistic measurements (PDF)

■ AUTHOR INFORMATION

Corresponding Author

*E-mail: lioz.etgar@mail.huji.ac.il.

ORCID

Qingbo Meng: 0000-0003-4531-4700

Lioz Etgar: 0000-0001-6158-8520

Notes

The authors declare no competing financial interest.

■ ACKNOWLEDGMENTS

We wish to acknowledge the Singapore National Research Foundation under the CREATE program: Nanomaterials for Energy and Energy-Water nexus and the Israel Science foundation NSFC-ISF Grant 2552/17. B.E.C. acknowledges the Israel Ministry of Infrastructure, Energy, and Water under the program for fellowships for Ph.D. students and the Rieger foundation fellowship for supporting her research.

■ REFERENCES

(1) Kojima, A.; Teshima, K.; Shirai, Y.; Miyasaka, T. Organometal Halide Perovskites as Visible-Light Sensitizers for Photovoltaic Cells. *J. Am. Chem. Soc.* **2009**, *131* (17), 6050–6051.

(2) Noh, J. H.; Im, S. H.; Heo, J. H.; Mandal, T. N.; Seok, S., Il Chemical Management for Colorful, Efficient, and Stable Inorganic-

DOI: 10.1021/acs.nanolett.9b00387
Nano Lett. 2019, 19, 2588–2597

Organic Hybrid Nanostructured Solar Cells. *Nano Lett.* **2013**, *13* (4), 1764−1769.
(3) Correa-Baena, J.-P.; Abate, A.; Saliba, M.; Tress, W.; Jacobsson, T. J.; Grätzel, M.; Hagfeldt, A. The Rapid Evolution of Highly Efficient Perovskite Solar Cells. *Energy Environ. Sci.* **2017**, *10*, 710.
(4) Burschka, J.; Pellet, N.; Moon, S. J.; Humphry-Baker, R.; Gao, P.; Nazeeruddin, M. K.; Grätzel, M. Sequential Deposition as a Route to High-Performance Perovskite-Sensitized Solar Cells. *Nature* **2013**, *499* (7458), 316−319.
(5) Lee, J. W.; Park, N. G. Two-Step Deposition Method for High-Efficiency Perovskite Solar Cells. *MRS Bull.* **2015**, *40* (8), 654−659.
(6) Kim, H. S.; Mora-Sero, I.; Gonzalez-Pedro, V.; Fabregat-Santiago, F.; Juarez-Perez, E. J.; Park, N. G.; Bisquert, J. Mechanism of Carrier Accumulation in Perovskite Thin-Absorber Solar Cells. *Nat. Commun.* **2013**, *4*, 1−7.
(7) Stranks, S. D.; Stranks, S. D.; Eperon, G. E.; Grancini, G.; Menelaou, C.; Alcocer, M. J. P.; Leijtens, T.; Herz, L. M.; Petrozza, A.; Snaith, H. J.; et al. Electron-Hole Diffusion Lengths Exceeding. *Science* **2013**, *342* (2013), 341−344.
(8) https://www.nrel.gov/pv/assets/images/efficiency-chart.png (date accessed November 2018).
(9) Mitzi, D. B. Templating and Structural Engineering in Organic-Inorganic Perovskites. *J. Chem. Soc. Dalt. Trans.* **2001**, No. 1, 1−12.
(10) Calabrese, J.; Jones, N.; Harlow, R.; Herron, N.; Thorn, D.; Wang, Y. Preparation and Characterization of Layered Lead Halide Compounds. *J. Am. Chem. Soc.* **1991**, *113* (6), 2328−2330.
(11) Ishihara, T. Optical Properties of PbI-Based Perovskite Structures. *J. Lumin.* **1994**, *60−61* (C), 269−274.
(12) Ishihara, T.; Hong, X.; Ding, J.; Nurmikko, A. V. Dielectric Confinement Effect for Exciton and Biexciton States in PbI4-Based Two-Dimensional Semiconductor Structures. *Surf. Sci.* **1992**, *267* (1−3), 323−326.
(13) Tanaka, K.; Takahashi, T.; Kondo, T.; Umebayashi, T.; Asai, K.; Ema, K. Image Charge Effect on Two-Dimensional Excitons in an Inorganic-Organic Quantum-Well Crystal. *Phys. Rev. B: Condens. Matter Mater. Phys.* **2005**, *71* (4), 1−6.
(14) Chernikov, A.; Berkelbach, T. C.; Hill, H. M.; Rigosi, A.; Li, Y.; Aslan, O. B.; Reichman, D. R.; Hybertsen, M. S.; Heinz, T. F. Exciton Binding Energy and Nonhydrogenic Rydberg Series in Monolayer WS2. *Phys. Rev. Lett.* **2014**, *113* (7), 1−5.
(15) Koutselas, I. B.; Ducasse, L.; Papavassiliou, G. C. Electronic Properties of Three- and Low-Dimensional Semiconducting Materials with Pb Halide and Sn Halide Units. *J. Phys.: Condens. Matter* **1996**, *8* (9), 1217−1227.
(16) He, X. F. Excitons in Anisotropic Solids: The Model of Fractional-Dimensional Space. *Phys. Rev. B: Condens. Matter Mater. Phys.* **1991**, *43* (3), 2063−2069.
(17) Tanaka, K.; Takahashi, T.; Ban, T.; Kondo, T.; Uchida, K.; Miura, N. Comparative Study on the Excitons in Lead-Halide-Based Perovskite-Type Crystals CH3NH3PbBr3CH3NH3PbI3. *Solid State Commun.* **2003**, *127* (9−10), 619−623.
(18) Mitzi, D. B. Solution-Processed Inorganic Semiconductors. *J. Mater. Chem.* **2004**, *14* (15), 2355−2365.
(19) Mitzi, D. B.; Feild, C. A.; Harrison, W. T. A.; Guloy, A. M. Conducting Tin Halides with a Layered Organic-Based Perovskite Structure. *Nature* **1994**, *369* (6480), 467−469.
(20) Knutson, J. L.; Martin, J. D.; Mitzi, D. B. Tuning the Band Gap in Hybrid Tin Iodide Perovskite Semiconductors Using Structural Templating. *Inorg. Chem.* **2005**, *44* (13), 4699−4705.
(21) Smith, I. C.; Hoke, E. T.; Solis-Ibarra, D.; McGehee, M. D.; Karunadasa, H. I. A Layered Hybrid Perovskite Solar-Cell Absorber with Enhanced Moisture Stability. *Angew. Chem., Int. Ed.* **2014**, *53* (42), 11232−11235.
(22) Cao, D. H.; Stoumpos, C. C.; Farha, O. K.; Hupp, J. T.; Kanatzidis, M. G. 2D Homologous Perovskites as Light-Absorbing Materials for Solar Cell Applications. *J. Am. Chem. Soc.* **2015**, *137* (24), 7843−7850.
(23) Quan, L. N.; Yuan, M.; Comin, R.; Voznyy, O.; Beauregard, E. M.; Hoogland, S.; Buin, A.; Kirmani, A. R.; Zhao, K.; Amassian, A.; et al. Ligand-Stabilized Reduced-Dimensionality Perovskites. *J. Am. Chem. Soc.* **2016**, *138* (8), 2649−2655.
(24) Tsai, H.; Nie, W.; Blancon, J. C.; Stoumpos, C. C.; Asadpour, R.; Harutyunyan, B.; Neukirch, A. J.; Verduzco, R.; Crochet, J. J.; Tretiak, S.; et al. High-Efficiency Two-Dimensional Ruddlesden-Popper Perovskite Solar Cells. *Nature* **2016**, *536* (7616), 312−317.
(25) Cohen, B.-E.; Wierzbowska, M.; Etgar, L. High Efficiency and High Open Circuit Voltage in Quasi 2D Perovskite Based Solar Cells. *Adv. Funct. Mater.* **2017**, *27* (5), 1604733.
(26) Cohen, B. E.; Wierzbowska, M.; Etgar, L. High Efficiency Quasi 2D Lead Bromide Perovskite Solar Cells Using Various Barrier Molecules. *Sustain. Energy Fuels* **2017**, *1* (9), 1935.
(27) Iagher, L.; Etgar, L. Effect of Cs on the Stability and Photovoltaic Performance of 2D/3D Perovskite-Based Solar Cells. *ACS Energy Lett.* **2018**, *3* (2), 366−372.
(28) Qing, J.; Liu, X. K.; Li, M.; Liu, F.; Yuan, Z.; Tiukalova, E.; Yan, Z.; Duchamp, M.; Chen, S.; Wang, Y.; et al. Aligned and Graded Type-II Ruddlesden−Popper Perovskite Films for Efficient Solar Cells. *Adv. Energy Mater.* **2018**, *8* (21), 1800185.
(29) Li, H.; Lu, J.; Zhang, T.; Shen, Y.; Wang, M. Cation Assisted Restraint of Wide Quantum Well and Interfacial Charge Accumulation in Two-Dimensional Perovskites. *ACS Energy Lett.* **2018**, *3*, 1815.
(30) Zhang, X.; Wu, G.; Fu, W.; Qin, M.; Yang, W.; Yan, J.; Zhang, Z.; Lu, X.; Chen, H. Orientation Regulation of Phenylethylammonium Cation Based 2D Perovskite Solar Cell with Efficiency Higher Than 11%. *Adv. Energy Mater.* **2018**, *8* (14), 1702498.
(31) Chen, Y.; Yu, S.; Sun, Y.; Liang, Z. Phase Engineering in Quasi-2D Ruddlesden-Popper Perovskites. *J. Phys. Chem. Lett.* **2018**, *9* (10), 2627−2631.
(32) Koh, T. M.; Shanmugam, V.; Guo, X.; Lim, S. S.; Filonik, O.; Herzig, E. M.; Müller-Buschbaum, P.; Swamy, V.; Chien, S. T.; Mhaisalkar, S. G.; et al. Enhancing Moisture Tolerance in Efficient Hybrid 3D/2D Perovskite Photovoltaics. *J. Mater. Chem. A* **2018**, *6* (5), 2122−2128.
(33) Fu, W.; Wang, J.; Zuo, L.; Gao, K.; Liu, F.; Ginger, D. S.; Jen, A.; Two-Dimensional, K.-Y. Perovskite Solar Cells with 14.1% Power Conversion Efficiency and 0.68% External Radiative Efficiency. *ACS Energy Lett.* **2018**, *3*, 2086.
(34) Zhang, X.; Ren, X.; Liu, B.; Munir, R.; Zhu, X.; Yang, D.; Li, J.; Liu, Y.; Smilgies, D. M.; Li, R.; et al. Stable High Efficiency Two-Dimensional Perovskite Solar Cells via Cesium Doping. *Energy Environ. Sci.* **2017**, *10* (10), 2095−2102.
(35) Wang, Z.; Lin, Q.; Chmiel, F. P.; Sakai, N.; Herz, L. M.; Snaith, H. J. Efficient Ambient-Air-Stable Solar Cells with 2D-3D Heterostructured Butylammonium-Caesium-Formamidinium Lead Halide Perovskites. *Nat. Energy* **2017**, *2* (9), 17135.
(36) Liao, J.-F.; Rao, H.-S.; Chen, B.-X.; Kuang, D.-B.; Su, C.-Y. Dimension Engineering on Cesium Lead Iodide for Efficient and Stable Perovskite Solar Cells. *J. Mater. Chem. A* **2017**, *5* (5), 2066−2072.
(37) Muljarov, E. A.; Tikhodeev, S. G.; Gippius, N. A.; Ishihara, T. Excitons in self-organized semiconductor/insulator superlattices: PbI-based perovskite compounds. *Phys. Rev. B: Condens. Matter Mater. Phys.* **1995**, *51* (14), 370−378.
(38) Saparov, B.; Mitzi, D. B. Organic-Inorganic Perovskites: Structural Versatility for Functional Materials Design. *Chem. Rev.* **2016**, *116* (7), 4558−4596.
(39) Atkins, P. *Physical Chemistry for the Life Sciences*; Oxford University Press: Oxford, U.K., 2006.
(40) Chang, R. *Physical Chemistry for the Biosciences*; Sausalito, 2005.
(41) Garrett, R. H. *Biochemistry*; Belmont, 2005
(42) Petrucci, R. H. et al. *General Chemistry*, 8th ed.; Prentice-Hall, Inc.: Upper Saddle River, NJ, 2002.
(43) Safdari, M.; Svensson, P. H.; Hoang, M. T.; Oh, I.; Kloo, L.; Gardner, J. M. Layered 2D Alkyldiammonium Lead Iodide Perovskites: Synthesis, Characterization, and Use in Solar Cells. *J. Mater. Chem. A* **2016**, *4* (40), 15638−15646.

DOI: 10.1021/acs.nanolett.9b00387
Nano Lett. 2019, 19, 2588−2597

(44) Nh, C. H.; Guan, J.; Tang, Z.; Guloy, A. M. A-$[NH_3(CH_2)_5NH_3]SnI_4$: A New Layered Perovskite Structure. *Mater. Sci. Forum* **1999**, *3*, 1833−1834.
(45) Mitzi, D. B.; Chondroudis, K.; Kagan, C. R. Design, Structure, and Optical Properties of Organic−Inorganic Perovskites Containing an Oligothiophene Chromophore. *Inorg. Chem.* **1999**, *38* (26), 6246−6256.
(46) Turren-Cruz, S.-H.; Hagfeldt, A.; Saliba, M. Methylammonium-Free, High-Performance and Stable Perovskite Solar Cells on a Planar Architecture. *Science (Washington, DC, U. S.)* **2018**, *3*, 362−449.
(47) Lee, J.-W.; Dai, Z.; Han, T.-H.; Choi, C.; Chang, S.-Y.; Lee, S.-J.; De Marco, N.; Zhao, H.; Sun, P.; Huang, Y. 2D Perovskite Stabilized Phase-Pure Formamidinium Perovskite Solar Cells. *Nat. Commun.* **2018**, *9*, 3021.
(48) Shpatz Dayan, A.; Cohen, B.-E.; Aharon, S.; Tenailleau, C.; Wierzbowska, M.; Etgar, L. Enhancing Stability and Photostability of $CsPbI_3$ by Reducing Its Dimensionality. *Chem. Mater.* **2018**, *30*, 8017.
(49) Zhang, T.; Dar, M. I.; Li, G.; Xu, F.; Guo, N.; Grätzel, M.; Zhao, Y. Bication Lead Iodide 2D Perovskite Component to Stabilize Inorganic α-CsPbI3 Perovskite Phase for High-Efficiency Solar Cells. *Sci. Adv.* **2017**, *3* (9), No. e1700841.
(50) Chen, J.; Seo, J.-Y.; Park, N.-G. Simultaneous Improvement of Photovoltaic Performance and Stability by In Situ Formation of 2D Perovskite at $(FAPbI_3)_{0.88}$ $(CsPbBr_3)_{0.12}$ /CuSCN Interface. *Adv. Energy Mater.* **2018**, *8* (12), 1702714.
(51) Zhu, X.; Podzorov, V. Extended Carrier Lifetimes and Diffusion in Hybrid Perovskites Revealed by Hall Effect and Photoconductivity Measurements. *Nat. Commun.* **2016**, 12253.
(52) Herz, L. M. Charge-Carrier Mobilities in Metal Halide Perovskites: Fundamental Mechanisms and Limits. *ACS Energy Lett.* **2017**, *2*, 1539.
(53) Saliba, M.; Correa-Baena, J.-P.; Wolff, C. M.; Stolterfoht, M.; Phung, N.; Albrecht, S.; Neher, D.; Abate, A. How to Make over 20% Efficient Perovskite Solar Cells in Regular (N−i−p) and Inverted (P−i−n) Architectures. *Chem. Mater.* **2018**, *30*, 4193.
(54) Li, M. H.; Yeh, H. H.; Chiang, Y. H.; Jeng, U. S.; Su, C. J.; Shiu, H. W.; Hsu, Y. J.; Kosugi, N.; Ohigashi, T.; Chen, Y. A.; et al. Highly Efficient 2D/3D Hybrid Perovskite Solar Cells via Low-Pressure Vapor-Assisted Solution Process. *Adv. Mater.* **2018**, *30* (30), 1801401.
(55) Unger, E. L.; Hoke, E. T.; Bailie, C. D.; Nguyen, W. H.; Bowring, A. R.; Heumüller, T.; Heumüller, H.; Christoforo, M. G.; Mcgehee, M. D. Hysteresis and Transient Behavior in Current-Voltage Measurements of Hybrid-Perovskite Absorber Solar Cells †. *Energy Environ. Sci.* **2014**, *7*, 3690.
(56) Kim, H.-S.; Jang, I.-H.; Ahn, N.; Choi, M.; Guerrero, A.; Bisquert, J.; Park, N.-G. Control of I−V Hysteresis in CH 3 NH 3 PbI 3 Perovskite Solar Cell. *J. Phys. Chem. Lett.* **2015**, *6*, 4633.
(57) Snaith, H. J.; Abate, A.; Ball, J. M.; Eperon, G. E.; Leijtens, T.; Noel, N. K.; Stranks, S. D.; Tse, J.; Wang, W.; Wojciechowski, K.; et al. Anomalous Hysteresis in Perovskite Solar Cells. *J. Phys. Chem. Lett.* **2014**, *5*, 1511.
(58) Eames, C.; Frost, J. M.; Barnes, P. R. F.; O'regan, B. C.; Walsh, A.; Islam, S.; Article, M. Ionic Transport in Hybrid Lead Iodide Perovskite Solar Cells. *Nat. Commun.* **2015**, *6*, 7497.
(59) Azpiroz, J. M.; Mosconi, E.; Bisquert, J.; De Angelis, F. Defect Migration in Methylammonium Lead Iodide and Its Role in Perovskite Solar Cell Operation †. *Energy Environ. Sci.* **2015**, *8*, 2118.
(60) Brivio, F.; Walker, A. B.; Walsh, A. Structural and Electronic Properties of Hybrid Perovskites for High-Efficiency Thin-Film Photovoltaics from First-Principles. *APL Mater.* **2013**, *1*, 042111.
(61) Frost, J. M.; Butler, K. T.; Brivio, F.; Hendon, C. H.; Van Schilfgaarde, M.; Walsh, A. Atomistic Origins of High-Performance in Hybrid Halide Perovskite Solar Cells. *Nano Lett.* **2014**, *14*, 2584.
(62) Duffy, N.; Peter, L.; Rajapakse, R. M.; Wijayantha, K. G. A Novel Charge Extraction Method for the Study of Electron Transport and Interfacial Transfer in Dye Sensitised Nanocrystalline Solar Cells. *Electrochem. Commun.* **2000**, *2* (9), 658−662.
(63) Misra, R. K.; Aharon, S.; Layani, M.; Magdassi, S.; Etgar, L. A Mesoporous-Planar Hybrid Architecture of Methylammonium Lead Iodide Perovskite Based Solar Cells †. *J. Mater. Chem. A* **2016**, *4*, 14423.
(64) Gottesman, R.; Lopez-Varo, P.; Gouda, L.; Jimenez-Tejada, J. A.; Hu, J.; Tirosh, S.; Zaban, A.; Bisquert, J. Dynamic Phenomena at Perovskite/Electron-Selective Contact Interface as Interpreted from Photovoltage Decays. *Chem.* **2016**, *1* (5), 776−789.
(65) Halme, J. Linking Optical and Electrical Small Amplitude Perturbation Techniques for Dynamic Performance Characterization of Dye Solar Cells. *Phys. Chem. Chem. Phys.* **2011**, *13* (27), 12435−12446.
(66) Peter, L. M.; Wijayantha, K. G. U. Electron Transport and Back Reaction in Dye Sensitized Nanocrystalline Photovoltaic Cells. *Electrochim. Acta* **2000**, *45* (28), 4543−4551.
(67) Aharon, S.; Dymshits, A.; Rotem, A.; Etgar, L. Temperature Dependence of Hole Conductor Free Formamidinium Lead Iodide Perovskite Based Solar Cells. *J. Mater. Chem. A* **2015**, *3* (17), 9171−9178.
(68) Zhao, Y.; Nardes, A. M.; Zhu, K. Solid-State Mesostructured Perovskite CH 3 NH 3 PbI 3 Solar Cells: Charge Transport, Recombination, and Diffusion Length. *J. Phys. Chem. Lett.* **2014**, *5* (3), 490−494.
(69) Cohen, B.; Aharon, S.; Dymshits, A.; Etgar, L. Impact of Antisolvent Treatment on Carrier Density in E Ffi Cient Hole-Conductor-Free Perovskite-Based Solar Cells. *J. Phys. Chem. C* **2016**, *120*, 142.
(70) Shi, J.; Zhang, H.; Xu, X.; Li, D.; Luo, Y.; Meng, Q. Microscopic Charge Transport and Recombination Perovskite Solar Cells. *Small* **2016**, *12* (38), 5288−5294.
(71) Shi, J.; Li, D.; Luo, Y.; Wu, H.; Meng, Q.; Shi, J.; Li, D.; Luo, Y.; Wu, H.; Meng, Q. Opto-Electro-Modulated Transient Photovoltage and Photocurrent System for Investigation of Charge Transport and Recombination in Solar Cells Opto-Electro-Modulated Transient Photovoltage and Photocurrent System for Investigation of Charge Transport and Re. *Rev. Sci. Instrum.* **2016**, *87*, 123107.
(72) Shi, J.; Li, Y.; Li, Y.; Luo, Y.; Wu, H.; Meng, Q.; et al. From Ultrafast to Ultraslow: Charge-Carrier Dynamics of Perovskite Solar Cells. *Joule* **2018**, *2* (5), 879−901.
(73) Giordano, F.; Abate, A.; Correa Baena, J. P.; Saliba, M.; Matsui, T.; Im, S. H.; Zakeeruddin, S. M.; Nazeeruddin, M. K.; Hagfeldt, A.; Graetzel, M. Enhanced Electronic Properties in Mesoporous TiO2 via Lithium Doping for High-Efficiency Perovskite Solar Cells. *Nat. Commun.* **2016**, *7*, 10379.

DOI: 10.1021/acs.nanolett.9b00387
Nano Lett. 2019, 19, 2588−2597